Acoustic Tractor Beam

Christine E. M. Démoré,[1] Patrick M. Dahl,[1,2] Zhengyi Yang,[1] Peter Glynne-Jones,[3] Andreas Melzer,[1] Sandy Cochran,[1] Michael P. MacDonald,[1,4,*] and Gabriel C. Spalding[2,†]

[1]*Institute for Medical Science and Technology, University of Dundee, 1 Wurzburg Loan, Dundee DD2 1FD, Scotland, United Kingdom*
[2]*Department of Physics, Illinois Wesleyan University, 201 East Beecher Street, Bloomington, Illinois 61701, USA*
[3]*Engineering Sciences, University of Southampton, University Road, Southampton SO17 1BJ, United Kingdom*
[4]*Division of Physics, University of Dundee, Nethergate, Dundee DD1 4HN, Scotland, United Kingdom*

(Received 18 August 2013; published 30 April 2014)

Negative radiation forces act opposite to the direction of propagation, or net momentum, of a beam but have previously been challenging to definitively demonstrate. We report an experimental acoustic tractor beam generated by an ultrasonic array operating on macroscopic targets (>1 cm) to demonstrate the negative radiation forces and to map out regimes over which they dominate, which we compare to simulations. The result and the geometrically simple configuration show that the effect is due to nonconservative forces, produced by redirection of a momentum flux from the angled sides of a target and not by conservative forces from a potential energy gradient. Use of a simple acoustic setup provides an easily understood illustration of the negative radiation pressure concept for tractor beams and demonstrates continuous attraction towards the source, against a net momentum flux in the system.

DOI: 10.1103/PhysRevLett.112.174302 PACS numbers: 43.25.Qp, 42.50.Wk, 43.20.El, 43.20.Fn

The momentum carried by fields and propagating waves has played a central role in the development of physics, impacting early discussions on the nature of light, the second law of thermodynamics, the Stefan-Boltzmann law, and the development of quantum mechanics [1]. The association of this momentum with "action at a distance" has intrigued humankind for centuries, yielding science fiction concepts such as the "tractor beam," in which an outflow of energy results, somewhat counterintuitively, in an influx of matter. By considering a general form of a tractor beam, theorists have recently proposed that attractive, or negative, forces can result from interactions of objects with directed optical and acoustic beams [2–11].

Some of the earliest experimental examples of remote manipulation with optical and acoustic fields took the form of levitation traps [12,13], using positive, nonconservative, radiation pressure from a beam to push objects away from the source and balance against gravity. A positive radiation force (F_+) is relatively intuitive and is in reaction to either backscattering or absorption of the forward-directed momentum of a beam and was famously reported in 1903 [14]. In contrast, most current optical and acoustic tweezing systems [15–18] are examples of conservative gradient force traps in which particles are drawn towards potential energy minima. However, tweezing systems that make use of potential energy wells do not provide the conceptual tractor beam defined in the theoretical literature, which is concerned with the role of (a negative) nonconservative radiation pressure, distinct from that of a gradient force, and directed towards the source. Time-evolving potential energy wells such as rotating anisotropic traps [19] or optical conveyors that move trapped particles by continuously sweeping potential energy minima [20,21] are also not examples of nonconservative forces and hence do not constitute a tractor beam under this definition. Examples of (positive) nonconservative forces in optics and acoustics include the transfer of orbital angular momentum [22–25] or guided transport along Bessel beams [26]. Specifically, it has been proposed that a tractor beam involves an attractive (negative) nonconservative force upon a target; that is, a continuous redirection of momentum flux is required [4–8].

With complex beams, including those with conical or helical phase fronts [2,8,27–30], there can be a substantial reduction of the axial component of the local Poynting vector. It is the forward redirection of this locally off-axis "skew" momentum by a scattering object that leads to a negative radiation force F_- on the object, even as the net momentum flux, or net Poynting vector, of the beam remains directed away from the source. Figure 1 illustrates such an arrangement and the concept of a tractor beam in its simplest form. Optical trapping systems demonstrating these principles have recently been reported, manipulating particles in the presence of a surface. In one approach, a tailored optical beam incident on microscopic particles in the presence of a reflecting surface produces both gradient and radiation forces; the targeted particles reach an equilibrium position where gradient forces balance a radiation pressure that is towards the virtual source [31]. In another approach, optical radiation forces opposing the projected axial momentum of an incident optical beam are exerted on particles situated at the interface between two different dielectric media when the beam is refracted towards the plane of the interface [32]. The experiment presented here

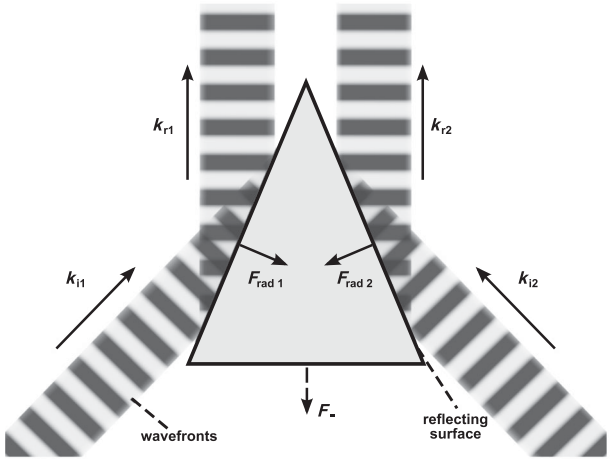

FIG. 1. Forward scattering of an acoustic or optical beam producing a net attraction force on a target. The change in momentum due to the axial redirection of a beam with locally off-axis components (k_{i1}, k_{i2}) by reflection or scattering (k_{r1}, k_{r2}) from the forward-facing surfaces of an object results in a radiation force F_{rad} with negative axial components and a resultant negative radiation force F_- towards the source and opposite to the net momentum flux of the beam.

demonstrates an acoustic negative radiation pressure directed towards the source, without the need for an additional reflecting surface or refractive interface. Moreover, since the region of F_- extends from the source, providing a continuous attraction against a net momentum flux in the system, it is compatible with bringing samples in, from a distance, to docking contact with a source. The acoustic tractor beam is demonstrated with macroscopic samples (here >1 cm) since acoustic devices can generate significantly larger forces (mN) than optical tweezers (pN) over larger length scales [25].

The present setup [33], illustrated in Fig. 2(a), uses a planar, 76-mm square aperture, ultrasonic matrix array operating at 550 kHz to form a directed acoustic field in a water-filled chamber. The ultrasound system and matrix transducer array used for the experiments (ExAblate 2100, InSightec, Tirat Carmel, Israel) is a clinically approved ultrasonic array system for MRI-guided focused ultrasound surgery [34,35] with individually controllable transducer elements. The authors have previously demonstrated, with this system, that complex pressure fields such as high-order helical beams [25] can be sculpted with appropriate control of the source aperture and phase profile. See Supplemental Material [33] for more information on the array control. Using the matrix array system, we steer locally planar wave fronts towards the axis of symmetry to produce an acoustic field with a sinclike cross-sectional profile in the absence of a target [Figs. 2(b)–2(d)]. That is, we have produced rectilinear analogs of the cylindrically symmetric conical wave fronts associated with the Bessel-like beams discussed in much of the literature on negative radiation forces [2–8,28–30]. This symmetric, rectilinear geometry

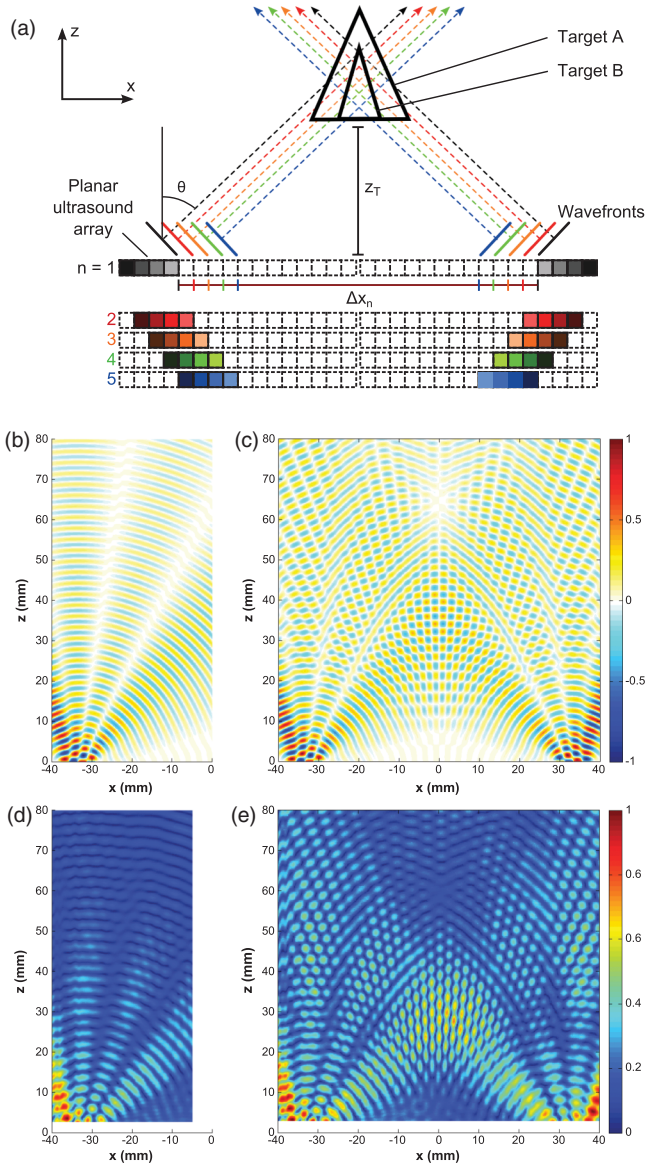

FIG. 2 (color). Experimental configuration to demonstrate negative radiation forces with a planar ultrasonic array. (a) Scaled cross-sectional geometry of the 550 kHz planar matrix array source and hollow, prism-shaped targets suspended above the array. Linear phase gradients applied to the array elements produce wave fronts steered at $\theta = 50.6°$ towards the array center line. Active subapertures, forming a hollow core with diameter Δx_n, are stepped towards the center line by the array element pitch, with a corresponding lateral ($\pm x$) shift in the transmitted local wave fronts and an axial ($-z$) shift of the intersection with the axis. (b),(c) Normalized maps of simulated instantaneous pressure field and (d),(e) measured magnitude of the pressure field produced by the transmitting subapertures illustrated under the field maps.

simplifies implementation and characterization of the acoustic fields and the associated target design and further demonstrates the ease with which negative radiation forces can be applied.

The phase profiles applied to the source array are designed to produce locally planar wave fronts steered at 50.6° from rectangular source apertures, symmetric about the array center line. By activating only a peripheral subset of the source array elements, we generate hollow-core beams with initial internal core size Δx. Simulated and measured maps of the pressure field transmitted from one side of the array [Figs. 2(b) and 2(d)] correspond well, showing the wave fronts steered at $\theta = 50.6°$ towards the center line and the grating lobe at 27° away from the center line, which does not interfere with the radiation force measurement. The simulated and measured interference patterns for the tractor beam in the absence of a target [Figs. 2(c) and 2(e)] show the expected distribution. As the pair of active apertures is stepped towards the center line, reducing Δx, the 50.6° steering angle and relative phases remain the same, and the region over which the wave fronts intersect moves closer to the source, as visualized in Movie S1 with Schlieren imaging [36].

In the presence of an appropriate target, scattering leads to redirection of the incoming wave, resulting in a continuous attractive force ($-\hat{z}$) towards the source when the beam intersects forward-facing sides of the target. Each target demonstrated here is a hollow isosceles triangular prism, extending the full length of the array, with an acoustic absorber on the base and thin metal sides to give large acoustic reflection coefficients. The targets were designed to demonstrate F_- and for mapping the force profile along the z axis shown in Fig. 2. Target A has an apex angle of 50°, approximately matching the steering angle to maximize the $+\hat{z}$ change in momentum of the beam, while target B has an apex angle of 38.2°, demonstrating that precise target geometry is not critical to the realization of F_- and is smaller, allowing more localized force measurement and profile mapping (see Supplemental Material [33]).

The net force on each target was measured directly as the excess or reduced weight on a balance from which the targets were suspended (see Supplemental Material [33]). A force balance is the standard method for determining the power generated by clinical ultrasound equipment, measuring the positive radiation pressure on a target in the beam. For each active aperture with separation Δx_n, the force profile was measured as a function of the target position above the source, z_T. Finite element analysis [37] was used both to predict F_{net} and to separate it into the component radiation forces on the target sides, F_-, and the base, F_+. Since acoustic velocity is not zero at all faces of the target, it is necessary to take this movement into account when calculating the mean force on the boundary. The net force on each surface was calculated via integration of the acoustic radiation stress tensor over the mean position of the surface of the target (see Supplemental Material [33]). Measured and predicted force profiles are compared in Fig. 3, and a simulation of the interaction between the acoustic pressure field and target B at different z_T is visualized in Movie S2.

The net steady state force depends simply on z_T and the cross section of the wave fronts incident on the target. When the field is turned on, the net lateral forces on the sides of the target cause it to shift and rotate so its length is parallel with the center line of the array, centering the target, no matter the initial lateral position. When the target is close to the array (small z_T), F_{net} is indeed negative, pulling it towards the array because the steered wave fronts primarily interact with target side surfaces. As z_T increases, the wave fronts begin to interact more with the absorbing base of the target and less with the sides, until F_+ and F_- are balanced [Fig. 3(a)]. When z_T is big enough, the wave fronts are incident primarily on the base, so F_{net} becomes positive, reaching a maximum upwards push when the base is at the highest intensity region of the field, before moving beyond the region of interference between the two crossing wave fronts. This same trend in forces is seen in both the simulation and experimental measurements and for both targets.

The wave fronts intersect the broader base of target A [Figs. 3(b) and 3(c)] at a lower z than target B [Figs. 3(b) and 3(d)], increasing the F_+ component, and consequently F_{net} is negative over a shorter distance from the source. However, the pulling force on target A is bigger, up to 1 mN, because of the larger surface area and optimized apex angle compared to target B. The difference in the ratio of the maximum upward and downward forces between the simulation and experiment can be attributed to a decrease in F_- from the nonunitary reflection coefficient at the sides and an increase in F_+ from reflections at the imperfectly absorbing base of the target. As expected, reducing Δx [Fig. 2(a)] has a similar effect to increasing z_T, such that the region, measured from the source, over which F_{net} is negative, is shorter. With larger Δx, the maximum of $|F_{\text{net}}|$ reduces because of diverging and lower intensity fields farther from the source, and the position of maximum negative radiation force is farther from the source. For both predicted and measured forces, the axial position z_{T0} at which $F_{\text{net}} = 0$ (Fig. 4) increases linearly with Δx, corresponding to an axial shift in the interference field of the tractor beam. Differences between the simulation and experiment can again be attributed to imperfect reflection and absorption by the targets. Above this position, the target is pushed away from the source, while below z_{T0} it is continuously pulled towards the source.

In this experiment, a phased array ultrasound source was used to apply a controllable negative radiation pressure that is continuous from the source until the directed beam diverges. The measured force profile confirms that the object is pulled towards the source even when the apex of the target intersects high intensity regions of the beam, demonstrating that the force is due to nonconservative radiation pressure, not a conservative force due to gradients

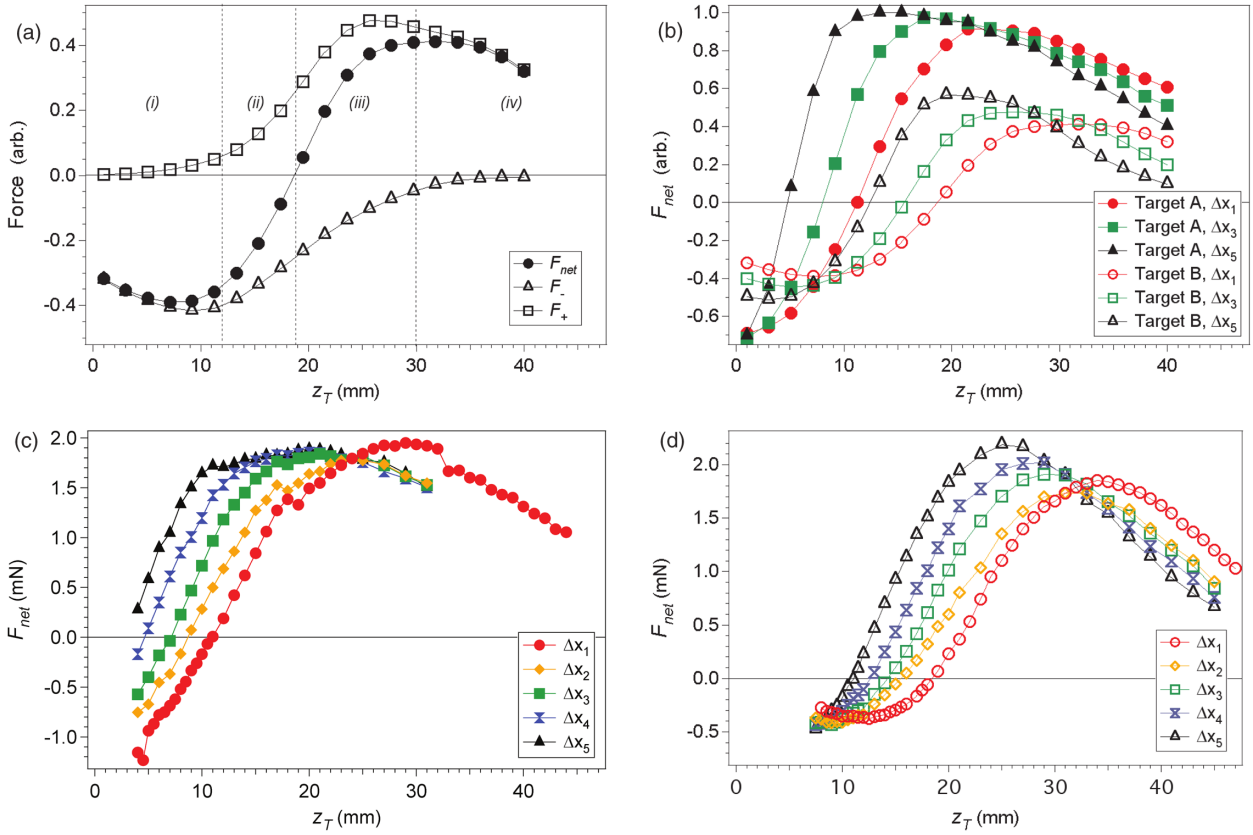

FIG. 3 (color online). Axial map of radiation forces on prism-shaped targets in tractor beams. (a) Predicted normalized net force profile F_{net} on target B by field transmitted from active subapertures with separation Δx_1. F_{net} is the sum of component vertical forces: positive radiation force F_+ due to absorption on the base and negative radiation force F_- from forward scattering at the target sides. Regions of interaction: (i) only the top of the target intersects the wave fronts, and F_{net} is minimized when wave fronts are maximally incident on target sides; (ii) wave fronts intersect more of the base and less of the sides until F_+ balances F_-; (iii) wave fronts are primarily incident on the absorbing base, increasing and then maximizing F_+; (iv) the target moves beyond the intersecting wave fronts and F_{net} decreases. (b) Predicted normalized net forces on target A and target B, with varying separation between active array subapertures, Δx_n. Measured net forces on (c) target A and (d) target B showing the same trend as the predicted forces. Target B begins with larger z_T because experimental considerations required a thicker absorbing base.

in the field. These results also indicate that these methods, in addition to other techniques, extend the dexterity of an ultrasonic matrix array to the point of having the ability to acoustically manipulate the position of matter in all directions, given the proper phasing and drive. Using the present 76-mm-wide ultrasonic array, F_- has been demonstrated for objects centered up to 29 mm away. This suggests that a large aperture source is required to manipulate distant objects but it will be possible to increase the net F_- with more tightly collimated beams, or more complex propagating beam types, such as Airy beams [38].

Negative radiation forces on objects, which arise from the reflection or scattering of locally off-axis wave fronts towards the beam axis, have been proposed for a range of particle trapping and manipulation applications using both optical and acoustic beams. We have demonstrated experimentally negative acoustic radiation forces on macroscopic objects. The use of a clinically approved ultrasound system opens up a range of potential medical and bioscience applications that may exploit tailored and complex ultrasound beams. By implementing the advanced control of ultrasound fields developed in experiments such as this, there is significant potential to improve the control of energy deposition in focused ultrasound surgery and targeted drug delivery, in which high intensity beams are used to treat tumors noninvasively. Negative radiation forces might also be used for in vivo manipulation and stimulation of objects, fluids, or biological tissue, yielding novel diagnostic techniques and treatment options. These, and other potential applications beyond the biomedical context in which the work was done, will benefit from the large forces possible with ultrasound, due to the long wavelength, and are not constrained to the simple target geometry used here. The depth penetration up to several centimeters we have achieved with the current ultrasound system is limited primarily by the discrete steering angles and the lateral extent of the current array. The approach demonstrated here provides additional incentives for

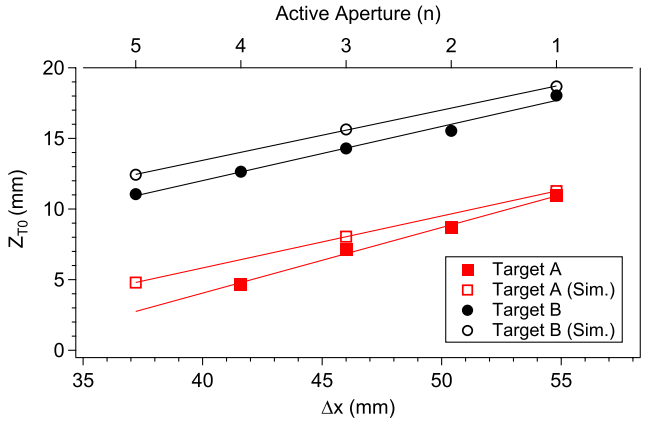

FIG. 4 (color online). Axial position of targets, z_{T0}, at which positive and negative radiation forces balance, calculated from the zero crossings in Fig. 3 for both simulation and experimental measurement of F_{net}.

developing tailored ultrasound fields for generating conservative and nonconservative forces and adds to the set of techniques available for contact-free, dexterous manipulation of objects.

This work has been funded by the Engineering and Physical Science Research Council, United Kingdom, through the Electronic Sonotweezers research project (EPSRC EP/G01213X/1); the European Community's Seventh Framework Program through the Nanoporation project (EU FP7 43915); and the European Regional Development Fund. M. P. M. acknowledges the support of the Scottish Funding Council. The authors thank A. Volovick of InSightec Ltd., Y. Qiu and Z. Qiu of the University of Dundee, and the Sonotweezers project partners at the Universities of Bristol and Glasgow for their support and assistance in this research. C. E. M. D. and P. M. D. contributed equally to this work.

*mikepmacdonald@gmail.com
†gspaldin@iwu.edu

[1] B. Carazza and H. Kragh, Annals of Science **46**, 183 (1989).
[2] P. L. Marston, J. Acoust. Soc. Am. **120**, 3518 (2006).
[3] F. G. Mitri and Z. E. A. Fellah, IEEE Trans. Ultrason. Ferroelectr. Freq. Control **55**, 2469 (2008).
[4] S. Sukhov and A. Dogariu, Opt. Lett. **35**, 3847 (2010).
[5] S. Sukhov and A. Dogariu, Phys. Rev. Lett. **107**, 203602 (2011).
[6] J. Chen, J. Ng, Z. Lin, and C. T. Chan, Nat. Photonics **5**, 531 (2011).
[7] A. Novitsky, C.-W. Qiu, and H. Wang, Phys. Rev. Lett. **107**, 203601 (2011).
[8] L. Zhang and P. L. Marston, Phys. Rev. E **84**, 035601 (2011).
[9] A. R. Zakharian, P. Polynkin, M. Mansuripur, and J. V. Moloney, Opt. Express **14**, 3660 (2006).
[10] J. Nemirovsky, M. C. Rechtsman, and M. Segev, Opt. Express **20**, 8907 (2012).
[11] A. Dogariu, S. Sukhov, and J. Sáenz, Nat. Photonics **7**, 24 (2012).
[12] A. Ashkin, Phys. Rev. Lett. **24**, 156 (1970).
[13] A. Ashkin and J. M. Dziedzic, Appl. Phys. Lett. **19**, 283 (1971).
[14] E. F. Nichols and G. F. Hull, Phys. Rev. (Series I) **17**, 26 (1903).
[15] A. Ashkin, J. M. Dziedzic, J. E. Bjorkholm, and S. Chu, Opt. Lett. **11**, 288 (1986).
[16] D. G. Grier, Nature (London) **424**, 810 (2003).
[17] K. C. Neuman and S. M. Block, Rev. Sci. Instrum. **75**, 2787 (2004).
[18] M. Evander and J. Nilsson, Lab Chip **12**, 4667 (2012).
[19] L. Paterson, M. P. MacDonald, J. Arlt, W. Sibbett, P. E. Bryant, and K. Dholakia, Science **292**, 912 (2001).
[20] T. Čižmár, V. Garcés-Chávez, K. Dholakia, and P. Zemánek, Appl. Phys. Lett. **86**, 174101 (2005).
[21] D. Ruffner and D. Grier, Phys. Rev. Lett. **109**, 163903 (2012).
[22] H. He, M. Friese, N. Heckenberg, and H. Rubinsztein-Dunlop, Phys. Rev. Lett. **75**, 826 (1995).
[23] J. Leach, S. Keen, M. J. Padgett, C. Saunter, and G. D. Love, Opt. Express **14**, 11919 (2006).
[24] K. Volke-Sepúlveda, A. Santillán, and R. Boullosa, Phys. Rev. Lett. **100**, 2 (2008).
[25] C. E. M. Demore, Z. Yang, A. Volovick, S. Cochran, M. P. MacDonald, and G. C. Spalding, Phys. Rev. Lett. **108**, 194301 (2012).
[26] H. Little, C. T. A. Brown, V. Garcés-Chávez, W. Sibbett, and K. Dholakia, Opt. Express **12**, 2560 (2004).
[27] N. B. Simpson, D. McGloin, K. Dholakia, L. Allen, and M. J. Padgett, J. Mod. Opt. **45**, 1943 (1998).
[28] P. L. Marston, J. Acoust. Soc. Am. **125**, 3539 (2009).
[29] F. G. Mitri, J. Phys. A **42**, 245202 (2009).
[30] L. Zhang and P. L. Marston, J. Acoust. Soc. Am. **131**, EL329 (2012).
[31] O. Brzobohatý, V. Karásek, M. Šiler, L. Chvátal, T. Čižmár, and P. Zemánek, Nat. Photonics **7**, 123 (2013).
[32] V. Kajorndejnukul, W. Ding, S. Sukhov, C.-W. Qiu, and A. Dogariu, Nat. Photonics **7**, 787 (2013).
[33] See Supplemental Material at http://link.aps.org/supplemental/10.1103/PhysRevLett.112.174302 for further details of the experimental setup, measurements and simulations.
[34] Y. Hertzberg, O. Naor, A. Volovick, and S. Shoham, J. Neural Eng. **7**, 056002 (2010).
[35] Y. Hertzberg and G. Navon, Med. Phys. **38**, 6407 (2011).
[36] G. S. Settles, *Schlieren and Shadowgraph Techniques* (Springer, Berlin, 2001).
[37] P. Glynne-Jones, P. P. Mishra, R. J. Boltryk, and M. Hill, J. Acoust. Soc. Am. **133**, 1885 (2013).
[38] K. Dholakia and T. Čižmár, Nat. Photonics **5**, 335 (2011).